Available online at www.sciencedirect.com
ScienceDirect
Microelectronic Engineering 85 (2008) 444–451
MICROELECTRONIC ENGINEERING
www.elsevier.com/locate/mee

Microstructure and dielectric response of $SrTiO_3/NdGaO_3$ interdigitated capacitors

Satreerat K. Hodak [a,*,1], Charles T. Rogers [b]

[a] Department of Physics, Chulalongkorn University, Bangkok 10330, Thailand
[b] Department of Physics, University of Colorado at Boulder, Boulder, CO 80309-0390, USA

Received 22 January 2007; accepted 17 August 2007
Available online 4 September 2007

Abstract

Epitaxial strontium titanate ($SrTiO_3$ or STO) thin films were prepared by an off-axis pulsed laser deposition technique on neodymium gallate ($NdGaO_3$ or NGO) substrates held at temperature of 820 °C. This technique allows different film growth rates in a deposition. Coplanar capacitors were fabricated and dielectric responses were measured at 1 MHz and at 2 GHz, and from 300 K to 4 K. The electric field tunability of the dielectric constant and loss tangent were taken with a range of electric field. The structure and morphology of the films were analyzed using high-resolution X-ray diffractometry and atomic force microscopy, respectively. The results showed that the films are crystalline with (1 0 0) orientation and the grains are columnar. Increased in-plane grain size and reduced surface to volume ratio were found to play a major role in improved performance of the film coplanar capacitors. The film with the growth rate of approximate 40 Å/min showed the highest change in the dielectric constant with an electric field of 4 V/μm. The film also showed the largest in-plane grain size of about 3000 Å.
© 2007 Elsevier B.V. All rights reserved.

Keywords: Strontium titanate; Dielectric properties; Grain size

1. Introduction

Strontium titanate ($SrTiO_3$ or STO) in its pure and unstressed form, is an incipient ferroelectric that has a number of interesting properties that are potentially useful in many applications. An incipient ferroelectric is a material that remains paraelectric down to 0 K, is not normally ferroelectric at any temperature, but shows a large increase in dielectric constant (ϵ_r) with decreasing temperature. This behavior is similar to what is seen in ferroelectrics when approaching the paraelectric to ferroelectric phase transition. Due to its matched lattice parameters and chemical compatibility with high temperature superconductors such as yttrium barium copper oxide ($YBa_2Cu_3O_{7-\delta}$ or YBCO), STO is ideal for use in YBCO/STO multilayer growth studies [1]. Undoped STO has applications in radio and microwave-frequency tunable capacitor devices particularly at low temperatures due to its high dielectric constant, low loss and the electric field tunability of its dielectric constant [2]. The main goal of improving the performance in these devices is to increase the tunability and decrease the dielectric loss at the same time, especially at microwave frequencies [1–3].

Thin films of STO show dramatic differences compared to the bulk. The dielectric constant of bulk STO increases nonlinearly from 300 at room temperature to 30,000 at 4 K with loss in the 10^{-3}–10^{-4} range. Between 4 K and 0.3 K, the bulk STO dielectric constant was found to be temperature independent due to the quantum-mechanical stabilization of the paraelectric phase [4]. On the other hand, STO thin films show a dielectric constant close to 300 at room temperature, which typically reaches a

* Corresponding author. Tel.: +66 2 218 7557; fax: +66 2 253 1150.
E-mail addresses: Satreerat.H@Chula.ac.th (S.K. Hodak), Charles.Rogers@colorado.edu (C.T. Rogers).
[1] Former address: Department of Physics, University of Colorado at Boulder, Boulder, CO 80309-0390, United States.

0167-9317/$ - see front matter © 2007 Elsevier B.V. All rights reserved.
doi:10.1016/j.mee.2007.08.007

maximum between 1000 and 10,000 in the 30–100 K range and then decreases steadily. STO thin films also show higher dielectric loss, typically in the range of 10^{-2}–10^{-3}. The high dielectric constant at low temperatures is associated with a low frequency transverse optical phonon mode or a soft mode, in which the oscillation of the Ti ion against the oxygen octahedral site is involved [5,6].

Most of the studies in STO polycrystalline and crystalline with a specific orientation have been made on different types of substrates such as Si, $SrRuO_3$ and $LaAlO_3$. In this article, we report the properties of epitaxy STO thin films grown by pulsed laser deposition on neodymium gallate ($NdGaO_3$) single crystal substrate with different growth rates in a deposition. We fabricated coplanar capacitors and measured dielectric properties as a function of temperature, frequency and electric field. We also characterized film structures, and investigated the correlation between their dielectric properties and crystal structures, and also their grain size. It has previously been found that the grain size has a major influence on the dielectric properties of thin films [7,8] and ceramic samples [9]. Normally, the growth temperature and annealing in oxygen atmosphere influence the film surface morphology and electrical properties [10]. With a fixed growth temperature, and also constant oxygen-annealing pressure, one of the variables that we found to profoundly affect the film properties is the film growth location with respect to the pulsed laser deposition plume. Structural and morphological variations of the STO/NGO films resulting from different deposition locations are reported for the first time.

2. Experimental details

We deposited strontium titanate thin films on neodymium gallate ($NdGaO_3$ or NGO) substrates by off-axis pulsed laser deposition technique [11]. The purpose of this experiment is to characterize the effects of growing films on NGO substrates mounted at different regions relative to the ablation plume axis, resulting in different film growth rates. The choice of the substrate was based on using low dielectric loss materials, with possibly minimum lattice mismatch with STO (lattice parameters: 3.905 Å for STO (1 0 0) and 3.86 Å for NGO (1 1 0), respectively, lattice mismatch: 1.1%). Other commercially available substrates such as $KTaO_3$ (3.989 Å), MgO (4.212 Å), and $LaAlO_3$ (3.79 Å) have larger lattice mismatches than that of NGO. Cleaned substrates were carefully mounted with colloidal silver on a 2 in. diameter heating stage, and placed in a vacuum chamber with a base pressure of 1×10^{-4} Pa before an oxygen pressure of 80 Pa was introduced. The temperature of the stage was slowly increased from room temperature to 820 °C. Fig. 1a shows the uniform temperature of substrates mounted across the heating stage. In our experimental setup, the heating stage is located 8.7 cm from the ablation target. A KrF excimer laser ($\sim$2 J/cm^2, 248 nm, 4 Hz) was focus with a 45 angle on a rotating STO target (single crystal, purity 99.9%. The oxygen pressure was maintained at 80 Pa and the temperature of the stage was kept at 820 °C during the film growth. These optimized growth conditions were obtained from previous studies in our laboratory [12]. After the growth, the films were cooled down under an oxygen pressure of 8×10^4 Pa. This was done because post-growth annealing treatments in oxygen atmosphere reduce oxygen vacancies in the films, minimizing the concentration of this type of defects [13,14]. During the annealing, the temperature was lowered to room temperature at a rate of 10 °C/min. Fig. 1b shows color[2] fringes on the heating stage after the film deposition. The plume axis intersects the stage surface at the point indicated by the cross. Ellipsometry was used to measure the film thickness, which varied depending on where the films were deposited relatively to the plume axis. The film growth rate was determined by the ratio of the measured thickness and the deposition duration as shown in Table 1. In order to perform dielectric function measurements, Ti/Au coplanar capacitor electrodes were fabricated with a 25 μm gap separation, 1.5 mm total gap width and with an overall 1×3 mm size using photolithography and evaporation techniques. A thin layer of Ti (200 Å) is evaporated on the sample before Au (3000 Å) because Au does not adhere very well on most substrates. The interdigital electrode coplanar capacitor is shown in Fig. 2a and b for cross sectional view and optical micrograph, respectively. Capacitance measurements were taken with LCR meter (HP 4275A) in the low frequency range and with network analyzer (HP 8510) for microwave frequencies using a previously described ring resonator technique [12,15].

3. Results and discussion

Fig. 3 shows the temperature dependence at 1 MHz of the dielectric constant and the loss for STO coplanar capacitors. The temperature range is from room temperature to 4 K. These films were grown under very similar conditions and differ primarily in their locations relative to the center of the laser ablation plume. The radial distance from where the plume center hits the heating stage is also presented in the Table 1. Separate studies of the local temperature variations on the heating stage indicated a uniform temperature distribution across the stage. Therefore, we attribute the differences in the films to differences in how and at what rates material is delivered to the substrate by the ablation plume. The growth rates increase as the films were deposited closer to the center of the ablation plume axis. In all cases (see Fig. 3a), the dielectric behavior of STO films is significantly different from that of the bulk (solid line) especially below 100 K. The dielectric constant for these films have a maximum between 30 and 60 K whereas that of the bulk increases monotonically down to 4 K. We note that films grown on NGO mounted at

[2] For interpretation of color in Fig. 1, the reader is referred to the web version of this article.

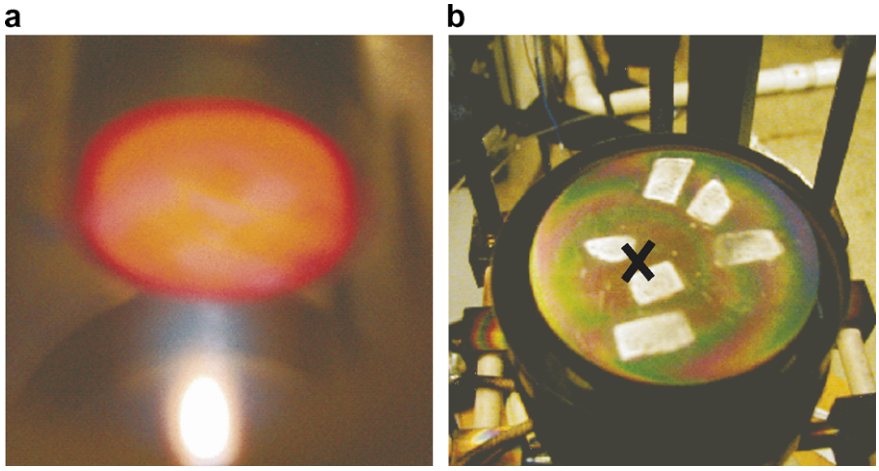

Fig. 1. (a) The uniform temperature of substrates mounted across the heating stage. (b) The color fringes on the heating stage after the film deposition (the cross indicates the plume axis).

Table 1
The characteristics of the studied films

Films	STO1	STO2	STO3	STO4
Distance from the plume axis (cm)	2.9	2.7	2.2	3.3
Peak ϵ_r (1 MHz)	3300	2600	1800	1000
Loss peak (1 MHz)	0.010	0.008	0.005	0.005
Growth rate (Å/min)	40	48	64	12
Thickness (ellipsometry) (Å)	4000	4800	6400	1200
Lattice parameter (XRD) (Å)	3.906	3.9057	3.913	3.916
In-plane grain size (AFM) (Å)	3100	2500	1400	1200
Tunability (4 K, 2 GHz) (%)	67	63	35	32
Average figure of merit (4 K, 2 GHz) (μm/V)	70	55	27	15
Grain boundary defects (%)	0.70	0.79	1.2	2.0

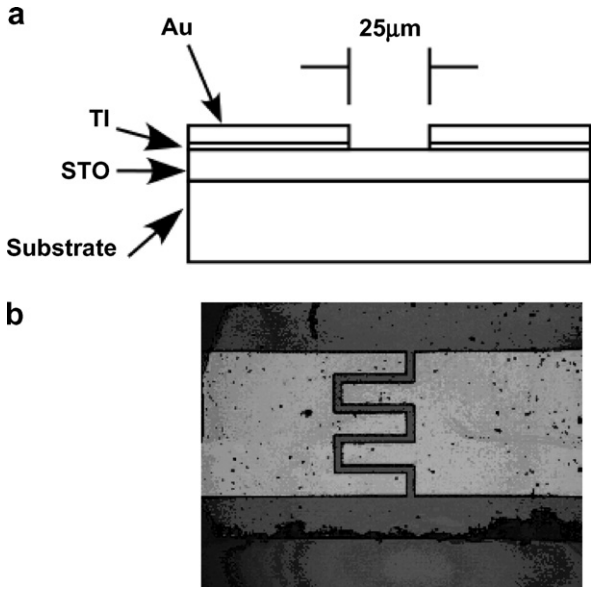

Fig. 2. Interdigitated coplanar capacitor. (a) Cross sectional view. (b) Optical micrograph of a finished coplanar capacitor.

2.9 cm and 2.7 cm far from the plume axis (STO1: open squares and STO2: open diamonds in Fig. 3, respectively) show the dielectric constant similar to that of the bulk STO from 75 K to room temperature. Other films grown on NGO mounted too close to the plume axis and too far from the plume axis (STO3: open triangle and STO4: cross, respectively) show deviations in the dielectric constant from that for bulk STO starting from 200 K to 4 K. Fig. 3b shows that the associated loss tangent is in the 0.005–0.03 range for our films, but it is less than 0.01 for bulk STO. Clearly the response of our capacitors in the MHz frequency can nearly match that for bulk STO if the films were grown at a certain region with respect to the ablation plume. We extended the measurement of dielectric response into the microwave frequency because many applications would require the use of STO films at that regime [1,15]. Fig. 4 shows the decreasing in maximum dielectric constant and increasing loss tangent of the best film (STO1) in microwave frequency measurement comparing with radio frequency measurements (at 10 kHz, 100 kHz, and 1 MHz). We observed two relaxation loss peaks around 50–70 K and 10 K, respectively. Viana et al. [6] have reported low frequency dielectric measurements on bulk STO, and observed two relaxation loss peaks around 100 K and 10 K, respectively. The high temperature loss peak indicates the phase transition from a cubic to a tetragonal structure [6]. Note that the loss peaks shift to higher temperature as the frequency of measure-

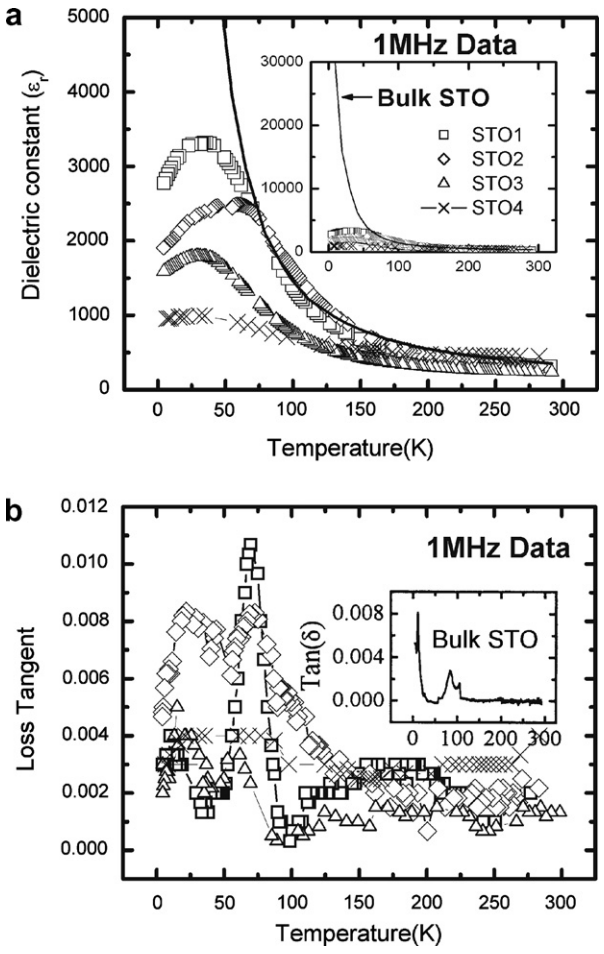

Fig. 3. (a) Dielectric function (ϵ_r) measured at 1 MHz as a function of temperature for films STO grown on NGO. For comparison, the solid line represents the bulk STO data. (b) Loss tangent at 1 MHz as a function of temperature for films STO grown on NGO.

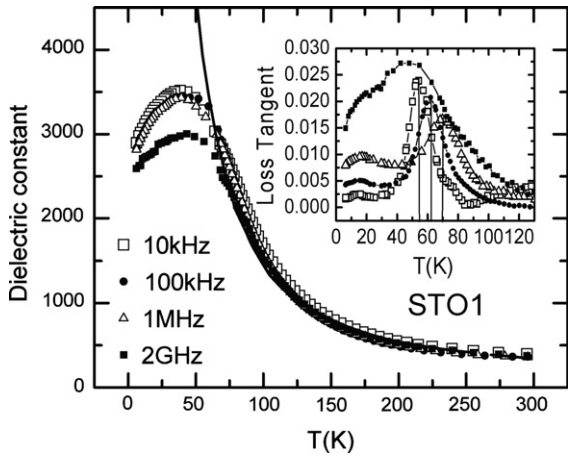

Fig. 4. Microwave frequency measurement comparing with 10 kHz, 100 kHz, and 1 MHz measurements of the STO1 film.

ment increases. This behavior suggests that dielectric losses are associated with thermally activated barriers. It is clearly seen that the high loss in ferroelectrics at microwave frequency limits the performance for devices. In the literature [16], a commonly used for determining the device performance, the figure of merit (K), is defined as the ratio of the tunability to the peak loss;

$$K = \frac{\varepsilon(E_0) - \varepsilon(E_{\max})}{\varepsilon(E_0)} \frac{1}{\tan \delta_{\max}} \tag{1}$$

where the tunability is given by the ratio between the change of dielectric constant when applying bias at the maximum and the dielectric constant at zero bias:

$$\text{Tuning} = \frac{\varepsilon(E_0) - \varepsilon(E_{\max})}{\varepsilon(E_0)} \tag{2}$$

However, it is difficult to compare the figure of merit of our films to those from other groups due to experimental factors such as the range of the applied electric field, the different temperature taken, and different measurement frequencies. Indeed, the K factor is temperature dependent as well as the tunability [16]. At room temperature, the dielectric responses of our strontium titanate thin films are independent of applied electric field indicating the paraelectric phase of the films. Fig. 5 shows the microwave measurements at 4 K of the dielectric constant and loss tangent tuning for applied electric fields in the range of 4 V/μm. The results of tuning and figure of merit (K) are

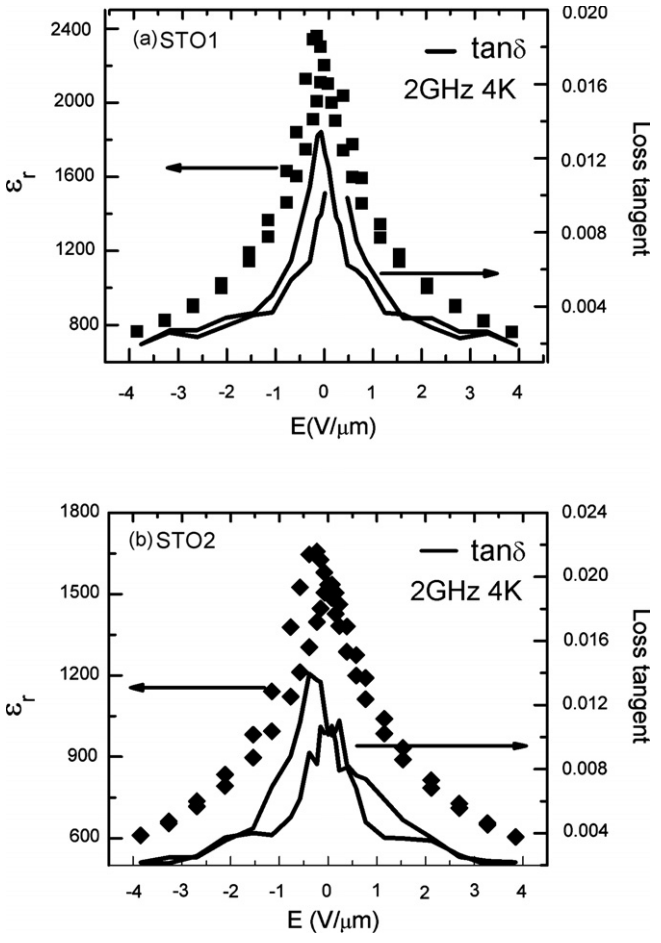

Fig. 5. The dielectric constant and loss tuning (at 2 GHz and 4 K) for applied electric fields in the range of 4 V/μm: (a) STO1 and (b) STO2.

presented in Table 1. STO1 and STO2 show a microwave loss peak below 0.015 while a large electric field tunability is maintained, resulting in high figure of merit of 70 μm/V and 55 μm/V, with high tunability of 67% and 63%, respectively. STO3 film which was grown at close to the plume axis shows low tunability of 35% resulting in low figure of merit of 27 μm/V. STO4 film grown too far from the plume axis shows lowest tunability of 32% and lowest figure of merit of 15 μm/V. The best film, STO1 was grown 2.9 cm measured from the ablation plume axis on the heating stage. We suggested that the optimum film growth rate of about 40 Å/min significantly enhances the dielectric performance of STO coplanar capacitor device.

3.1. Characterization of the film structure

It is desirable to establish how the films grown under different growth rates differ from a structural point of view. Furthermore, given the wide variety of dielectric behavior, we expect to find strong correlations between the dielectric properties and the internal film structure. We have therefore carried out a series of high resolution X-ray diffraction experiments to investigate these issues. Specially, we studied the correlation between the dielectric properties of these films and their crystal structure and microstructure using X-ray diffraction and atomic force microscopy, respectively. We performed the high resolution X-ray measurements with a synchrotron diffraction beamline ($\lambda = 1.55857$ Å) [17]. Our STO films have preferential [1 0 0] growth perpendicular to the surface of the (1 1 0) NGO substrates. Fig. 6a and b show the data obtained with synchrotron radiation for the first order (1 0 0) diffraction pattern for STO films grown on NGO. The data shown in Fig. 6a corresponds to the film STO1 prepared away from the plume axis and with a correspondingly high dielectric constant and low loss. The high symmetry of the peak and the presence of fringes are indicative of high crystallinity, uniform layer and low strain [18]. The narrow peak suggests that the film STO1 (FWHM = 0.025°) has very low concentration of defects [19]. In contrast, the film STO3 (FWHM = 0.035°) (see Fig. 6b) grown near the plume center displays clearly asymmetrical and wider diffraction patterns. Crystal imperfections such as the out-of-plane lattice strain, in-plane strain (mismatch with the substrate), point defects, line defects and volume defects can also contribute to the observed asymmetric shapes [20]. The line in Fig. 6 is the best fit provided by the Rietveld method [21] using the Generalized Structure and Analysis Software (GSAS) package [22]. The residuals are shown in the bottom curve in Fig. 6. The peaks were modelled by a Pseudo Voigt function [22] with the assumption of a cubic point group for STO [23]. The refined lattice parameters are presented in Table 1. We found that in all cases the crystallite size in a direction perpendicular to the plane of the film (out-of-plane grain size) is consistent with the film thickness obtained from our ellipsometry measurements indicating the columnar grains.

The microstructure of the films such as grain size, disorder, pores and boundary defects can be seen in the atomic force microscopy images. Fig. 7 shows atomic force microscopy (AFM) 2 × 2 μm images of the STO thin films. The in-plane grain size of these films is in the 1000–3000 Å range, slightly larger than the in-plane grain size of STO thin films reported in literature [12,24,25] which is in 500–2000 Å range. For comparison, the grain size in STO ceramics is in the 1–50 μm range [24]. Fig. 7 show that the film STO3 prepared close to the plume axis have smaller grain sizes than that of the films grown at far from the plume axis STO1 and STO2. Fig. 7d shows the surface of the STO4 film having a thickness only 1000 Å. The in-plane grain size of this film is small compared to other films in Fig. 7 even though it was grown far from the plume. This suggests that for the columnar type of growth observed in our films there is a minimum aspect ratio that is necessary to grow a large

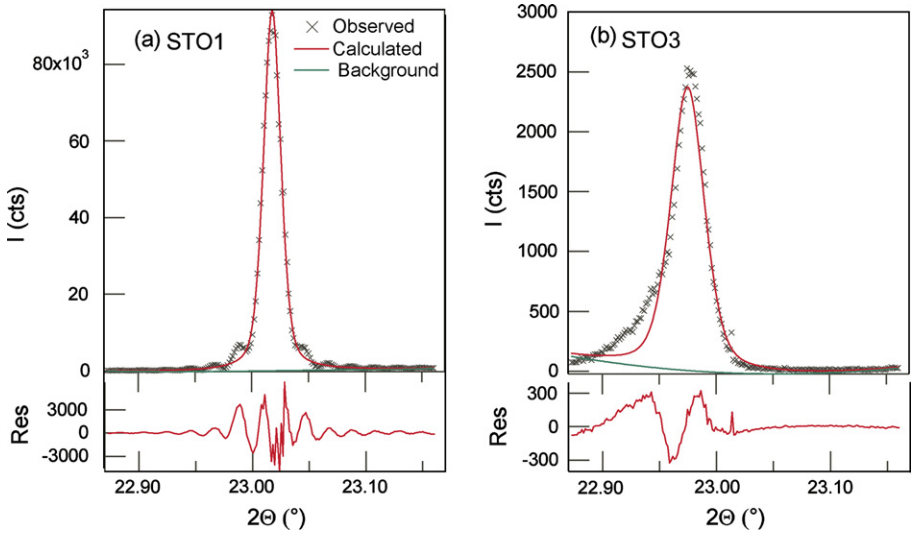

Fig. 6. High resolution X-ray diffraction ($\lambda = 1.55857$ Å) on the (1 0 0) STO films: (a) STO1 and (b) STO3.

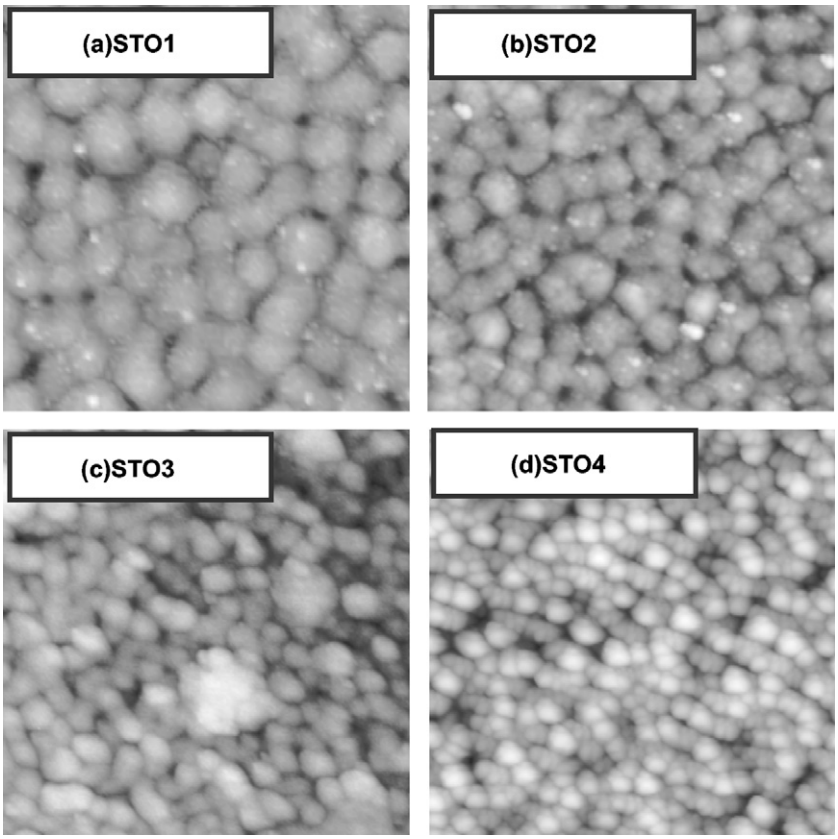

Fig. 7. The 2 μm × 2 μm atomic force microscope images of the strontium titanate films: (a) STO1, (b) STO2, (c) STO3 and (d) STO4.

crystal. The film STO4 lies below such crystallization onset, and thus it is too thin to form large grains. One possible reason for this behavior is the presence of strain in the crystallites due to the lattice mismatch with the substrate. Indeed, complete strain relaxation of the STO film takes place at film thickness in the 500–2500 Å range depending on the deposition temperature [26].

The observed columnar growth suggests that strain inducing defects at the boundary between grains may be formed due to differences in the growth rate between neighboring columns. Film–substrate lattice mismatch is known to introduce strain on the films. [26,27] The release of the strain by lift off was shown to reduce the loss without an appreciable change in the dielectric constant [27]. We speculate that the strain between the film–substrate and between the grains play a major role in determining the dielectric constant and loss of the films.

The proportion of grain boundary defects in the crystallites will scale with the surface to volume ratio of the grains. The smallest possible defect containing entity is a unit lattice cell. Thus, the proportion of defects should scale with the ratio of the number of surface cells to the total number of lattice cells in the grain. Assuming a cylindrical shape for the columnar grains, the volume of each grain is simply $V = \pi r^2 t$ where r is the radius of a grain and t is the film thickness. The area of the grains is estimated as $A = \pi r^2 + \pi r^2 + 2\pi r t$. We thus estimate the fraction of defects containing unit cells as

$$\text{Number of surface cells} = \frac{A}{(a \times a)} \tag{3}$$

where a is a lattice constant for STO films (see Table 1). The total number of volume cells in the cylindrical grain is given by

$$\text{Number of volume cells} = \frac{V}{(a \times a \times a)} \tag{4}$$

The maximum percentage of boundary defects is given by the number of surface cells divided by the total number of volume cells.

$$\text{Boundary defect}(\%) = \frac{\text{Number of surface cells}}{\text{Number of volume cells}} \times 100 \tag{5}$$

The calculated percentage of boundary defects for our films are shown in Table 1.

In Fig. 8, the figure of merit for studied films at 4 K and 2 GHz is plotted with the in-plane grain size and the boundary defects. The STO1 film with highest figure of merit shows the highest in-plane grain size and the lowest boundary defect. The data shows a nearly linearly proportional dependence of the figure of merit with the in plane grain size. Extrapolation of this trend to zero grain size yields zero figure of merit within the error bars, as expected for this limit. Interestingly a similar limit is found for barium titanate nanoparticles (average diameter of 30 nm) for

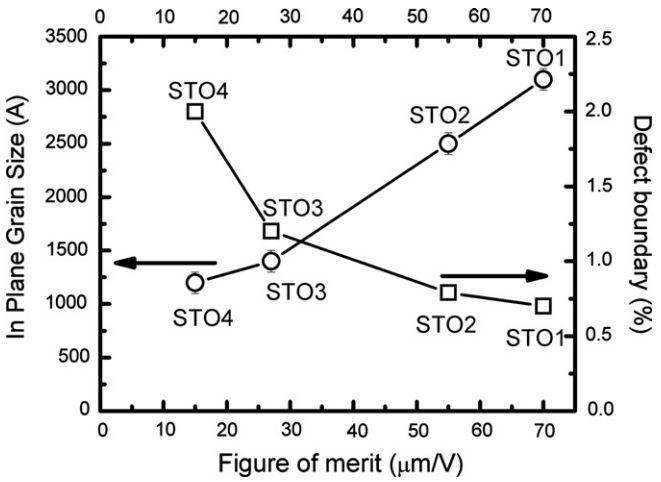

Fig. 8. Plot of grain size, boundary defect and figure of merit as described in the text.

which the ferroelectric behavior is prevented because these crystals are not large enough to have more than one ferroelectric domain [8]. There have been previous reports showing strong correlation between grain size and dielectric constant. For STO films on lanthanum aluminate, Dalberth et al. found that the films with large static dielectric function also have larger grain size [12]. Our best STO/NGO film obtained from off-axis growth show improved dielectric performance, with a figure of merit at least two times larger than that of the free-standing films [27]. A pronounced correlation was also found between the dielectric boundary and the grain size for diamond films [28] and for barium titanate films [7]. Clearly in plane grain size has a major impact on the figure of merit for our coplanar capacitors. In contrast, the performance for our fabricated capacitors does not depend on the out of plane grain size. This could be due to the direction of applied electric field parallel to the in plane grain size. The rms roughness for our films was in the 2–5 nm range which is less than 3% of the thickness for all of our films and on the order of the roughness of the bare substrate which is approximately 1 nm. Thus, we concluded that the observed variations in figure of merit are not due to differences in the roughness among our films.

A recently published article showed that thermal cycling in oxygen rich atmosphere increased the dielectric properties of the films [29]. Interestingly such oxygen treatments improved the figure of merit at the MHz frequency, but not in the GHz range. The result of our experiments provide an important insight towards how to improve the quality of STO films at MHz and GHz frequencies. It is expected that a slow rate of material delivery by the plume in the deposition process will tend to provide the largest in plane grain size producing films with low loss and high dielectric constant. No clear correlation between the lattice parameters of the films and the figure of merit can be concluded from our data set, which is consistent with the results of other studies [30].

4. Conclusions

STO films have been grown by off-axis pulsed laser deposition on NGO single crystal substrates, at 820 °C and oxygen pressure of 80 Pa. The STO/NGO film with the growth rate of approximate 40 Å/min, the largest in-plane grain size, and the smallest grain boundary defects showed the highest figure of merit of 70 μm/V at 2 GHz and 4 K, and a change in the dielectric constant of 67% with an electric field of 4 V/μm. The morphology of the films and their dielectric behavior are strongly dependent on the position of the substrate relative to the plume axis as well as the film growth rate. The correlation of dielectric performance in our coplanar capacitor and in-plane grain size and percentage of defects could be useful in controlling the quality of the films. We have found that in-plane grain size is the most important factor determining the dielectric performance of film coplanar capacitors.

Acknowledgements

This research was partially funded by the Office of Naval Research. We gratefully acknowledge J.C. Price and M.J. Dalberth for the discussion. The authors would like to thank D. Balzar, D.A. Coleman, and C. Jones for their help in the X-ray analysis.

References

[1] A.T. Findikoglu, C. Doughty, S.M. Anlage, Q. Li, X.X. Xi, T. Vankatesan, J. Appl. Phys. 76 (1994) 2937.
[2] H.M. Christen, J. Mannhart, E.J. Williams, C. Gerber, Phys. Rev. B 49 (17) (1994) 12095–12104.
[3] D. Galt, J.C. Price, J.A. Bealle, R.H. Ono, Appl. Phys. Lett. 63 (22) (1993) 3078–3080.
[4] K.A. Muller, H. Burkard, Phys. Rev. B 19 (7) (1979) 3593–3602.
[5] R.A. Cowley, Phys. Rev. Lett. 9 (1962) 159.
[6] R. Viana, P. Lunkenheimer, J. Hemberger, R. Bohmer, A. Loidl, Phys. Rev. B 50 (1994) 601–604.
[7] C. Fu, C. Yang, H. Chen, L. Hu, Y. Wang, Mater. Lett. 59 (2005) 330–333.
[8] K. Suzuki, K. Kijima, Vacuum 80 (2006) 519.
[9] H.T. Martirena, J.C. Burfoot, J. Phy. C: Solid State Phys. 7 (1974) 3182–3192.
[10] X. Wang, S. Olafsson, P. Sandstrom, U. Helmersson, Thin Solid Films 360 (1999) 181–186.
[11] S. Kampangkeaw, C.T. Rogers, in: Materials Issues for Tunable RF and Microwave Devices III, Materials Research Society Symposium Proceedings, USA, H2.5.1-H2.5.5 (2002) 720.
[12] M.J. Dalberth, R.E. Stauber, J.C. Price, C.T. Rogers, Appl. Phys. Lett. 72 (4) (1998) 507–509.
[13] M. Sirena, N. Haberkorn, M. Granada, L. Steren, J. Guimpel, J. Magn. Mater. 272–276 (1) (2004) 1171–1173.
[14] W. Chang, J.S. Horwitz, A. Carter, J.M. Pond, S. Kirchoefer, C.M. Gilmore, D. Chrisey, Appl. Phys. Lett. 74 (1999) 1033.
[15] D. Galt, J. Price, J.A. Beall, T.E. Harvey, IEEE Trans. Appl. Supercond. 5 (1995) 2575.
[16] H.-C. Li, W. Si, A.D. West, X.X. Xi, Appl. Phys. Lett. 73 (1998) 190–192.
[17] The National Synchrotron Light Source, Brookhaven National Laboratory, New York (Beam line X10A).
[18] R.W. James, The Optical Principles of the Diffraction of X-rays, G. Bell and Sons Ltd., London, 1958.

[19] D. Balzar, P.A. Ramakrshnan, P. Spagnol, S. Mani, A.M. Hermann, M.A. Matin, Jpn. J. Appl. Phys. 41 (2002) 6628–6632.
[20] D. Hull, D. Bacon, Introduction to Dislocations, Butterworth Heinemann, UK, 2001.
[21] H.M. Rietveld, Acta Crystallogr. 22 (1967) 151–152.
[22] B.H. Toby, J. Appl. Crystallogr. 34 (2001) 210–213.
[23] International Table for X-ray Crystallography, Kynoch Press, for the International Union of Crystallography, Birmingham, England, 1952–1974.
[24] T. Ostapchuk, J. Petzelt, V. Zelezny, A. Pashkin, J. Pokorny, I. Drbohlav, Phys. Rev. B 66 (23) (2002) 235406(1)–235406(12).
[25] Y. Gao, Y. Masuda, T. Yonezawa, K. Koumoto, Mater. Sci. Eng. B99 (2003) 290–293.
[26] L.S.-J. Peng, X.X. Xi, B.H. Moeckly, S.P. Alpay, Appl. Phys. Lett. 83 (22) (2003) 4592–4594.
[27] M.J. Dalberth, J.C. Price, C.T. Rogers, in: Ferroelectric Thin Films VI, Materials Research Society Symposium Proceedings, USA, 493 (1998) 371.
[28] H. Ye, C.Q. Sun, P. Hing, J. Phys. D 34 (2001) 148.
[29] P.K. Petrov, N.M. Alford, Appl. Phys. Lett. 87 (2005) 222902.
[30] R.E. Treece, J.B. Thompson, C.H. Mueller, T. Rivkin, M.W. Cromar, IEEE Trans. Appl. Supercond. 7 (2) (1997).